

Neglecting uncertainty can lead to failing stormwater infrastructures

Sanjib Sharma^{1*}, Ben Seiyon Lee², Robert E. Nicholas^{1,3}, Klaus Keller^{1,4}

¹Earth and Environmental Systems Institute, The Pennsylvania State University, University Park, PA, USA

²Department of Statistics, The George Mason University, Fairfax, VA, USA

³Department of Meteorology and Atmospheric Science, The Pennsylvania State University, University Park, PA, USA

⁴Department of Geosciences, The Pennsylvania State University, University Park, PA, USA

*Corresponding author

Keywords:

Extreme Precipitation, Flood Risk, Stormwater Infrastructure Design, Climate Change, Decision-Making under Deep Uncertainty

Abstract

Current approaches to design stormwater infrastructure typically assume a stationary rainfall distribution and neglect many uncertainties. These assumptions are inconsistent with observations that suggest intensifying extreme precipitation events and the uncertainties surrounding projections of the coupled natural-human systems. Here we show that assuming climate stationarity and neglecting deep uncertainties can drastically underestimate flood risks and lead to poor infrastructure design choices. We find that climate uncertainty dominates the socioeconomic and engineering uncertainties that impact the hydraulic reliability in stormwater drainage systems. We quantify the upfront costs needed to achieve higher hydraulic reliability and robustness against the deep uncertainties surrounding projections of rainfall, surface runoff characteristics, and infrastructure lifetime. Depending on the location, we find that adding safety factors of 1.4 to 1.7 to the standard stormwater pipe design guidance produces robust performance to the considered deep uncertainties.

Main

Floods drive devastating climate-related impacts and human disasters¹. Average global flood losses exceed US\$100 billion per year². Model simulations project rising flood risks with intensifying climate change and increasing exposure^{3,4}. A sound understanding of the transient flood risk and proper tools to account for the risk-dynamics are crucial to inform flood-risk management^{1,5,6}.

Engineers and decision makers around the world face nontrivial choices on how to design flood-sensitive infrastructure such as stormwater drainage systems. Current guidelines for this decision problem^{7,8} typically consider the observed historical record and assume a stationary climate (i.e., assumes statistical properties of extremes do not change significantly over the design lifetime)⁹⁻¹². This stationary rainfall assumption is inconsistent with the observed record in many parts of the world¹⁰. Moreover, rainfall extremes are projected to intensify further in a warming climate¹³. In addition, neglecting climate change violates a recent executive order in the United States¹⁴. This raises the question: How to design stormwater infrastructure in a nonstationary world?^{10,11}

Current infrastructure design specifications typically neglect key uncertainties surrounding projections of extreme rainfall and surface runoff during infrastructure lifetime¹⁵. Deep uncertainty surrounding rainfall projections stems, for example, from internal variability, model limitations such as unresolved processes and coarse spatio-temporal resolutions, as well as uncertainties surrounding land use change and greenhouse gas emissions scenarios¹⁶. Deep uncertainty refers to a situation “where the system model and the input parameters to the system model are not known or widely agreed on by the stakeholders to the decision”¹⁷. In infrastructure design, for example, deep uncertainty might arise when experts and/or decision-makers cannot agree on an appropriate probability density function for describing extreme rainfall projections or a return level

corresponding to a particular design return period¹⁸. Uncertainties surrounding surface runoff characteristics and the project lifetime further complicate the situation¹⁹.

Previous studies^{9,11,20,21} provide valuable new insights on the impacts of climate change on the design and performance of flood-sensitive infrastructures. For example, Wright *et al.*¹¹ demonstrates that the current hydrologic design standards in the United States are insufficient due to substantial increases in extreme rainfall frequency. Mallakpour *et al.*²⁰ shows that the hydrologic failure risk is likely to increase for most dams in California under various warming scenarios. Cook *et al.*²¹ analyzes how the choices in climate model spatial resolution and spatial adjustment technique alter the size of urban stormwater drainage. These studies break important new ground, but they are silent on the effects of potentially important uncertainties and their interactions^{22,23}. Here we expand on these studies by (i) characterizing the uncertainty surrounding the project lifetime, runoff characteristics, and nonstationary extreme rainfall projections, (ii) identifying their interacting effects and relative importance on system performance, and (iii) quantifying the implications of these uncertainties for the design of stormwater infrastructure (Fig. 1).

Specifically, we select three locations from diverse hydroclimatic regions in the United States: i) Ellicott City (Maryland), ii) Boulder (Colorado) and iii) Los Angeles (California). These locations have experienced several severe flooding events over the recent decades²⁴ and sample diverse meteorological settings. Examples include floods associated with localized cloudbursts from clusters of intense thunderstorms in Ellicott City (2016 and 2018)²⁵, heavy rainfall driven floods in Boulder (2013)²⁶, and prolonged rainfall induced floods over California in 2017 immediately after 5 years of record-setting drought²⁷. We use the daily rainfall records²⁸ from gauge stations at the Baltimore/Washington International Thurgood Marshall Airport (Maryland), Boulder Municipal Airport (Colorado), and Los Angeles International Airport (California) (Supplementary Table S1).

We demonstrate the approach for a simple didactic decision problem: how to choose a stormwater pipe size in the face of deeply uncertain projections of extreme rainfall, surface runoff characteristics, and infrastructure lifetime (Fig. 2).

Results

We first quantify the deep uncertainty surrounding extreme rainfall projections. Specifically, we estimate extreme rainfall from the historical rainfall record under the stationary assumption using a Generalized Extreme Value distribution within the Bayesian framework (see Methods Section). We find that neglecting parametric uncertainty (i.e., uncertainty associated with fitting a parametric distribution to historical data) underestimates the expected value of projected extreme rainfall events (Supplementary Figs. 1b-c). Using just the best estimate of the model parameters (technically the maximum *a posteriori* probability estimate) underestimates the extreme rainfall projections by as much as 8% (Supplementary Figs. 1b-c) compared to an analysis that resolves the parametric uncertainty. This effect is driven by the right-skewed return level distribution (Supplementary Fig. 1b) and similar to related analyses on riverine flooding²⁹. The downward bias increases for longer return periods. This bias can drive higher flood infrastructure failure risks.

Previous studies³⁰⁻³² show that the sea surface temperature variability has a strong influence on the variability of atmospheric climate through atmospheric teleconnections. Following previous research^{6,33,34}, we construct nonstationary statistical model that allows integrating relevant physical drivers of extreme rainfall as covariates (Fig. 3): global mean surface temperature, local surface temperature, Atlantic main development region temperature³⁵, North Atlantic Oscillation index³¹, Pacific Decadal Oscillation index³⁶, Nino 3.4 index³⁷, and Southern Oscillation index³⁰. We use the Akaike information³⁸ and Deviance information³⁹ criteria (AIC and DIC) to identify the best model structure and covariate that fits the observed rainfall dataset. Our analysis suggests that the extreme

rainfall distribution in Ellicott City reflects a greater contribution from the average sea surface temperature in the Atlantic main development region³⁵ (Supplementary Table S2). The Atlantic main development region (10⁰N-20⁰N, 80⁰W-20⁰W) is monitored for potential tropical system development regions during the course of a given Atlantic hurricane season. For the observed rainfall distribution in Boulder, local temperature emerges as the best covariate choice. We estimate extreme rainfall intensity in Los Angeles by taking advantage of the dependence relationship in the time series of the Nino 3.4 index and historical rainfall observations. Previous studies^{40,41} suggest that the Nino 3.4 average sea surface temperature anomalies in the area of tropical Pacific Ocean (5°S–5°N, 120°–170°W) has a substantial influence on precipitation in many parts of California.

Accounting for nonstationarity increases the mean estimates of extreme rainfall intensity (Figs. 3a, c, e). For example, the current mean estimate of the 24-hour average rainfall intensity with a 100-year return period increases by roughly 2.9 mm/hr in Boulder (Fig. 3c). The increase in current mean extreme rainfall estimates increase with longer return periods. As perhaps expected, the uncertainty also increases with longer return periods. Assuming a stationary rainfall distribution for infrastructure design can lead to poor outcomes (Figs. 3a, c, d). For a historical rainfall event with a stationary expected return period of 100-years, the corresponding return periods under nonstationary conditions reduces to 78 years in Ellicott City (Fig. 3a), 60 years in Boulder (Fig. 3c), and 90 years in Los Angeles (Fig. 3e).

The extreme rainfall projections are deeply uncertain (Figs. 3b, d, f). We represent this deep uncertainty by sampling from a set of (i) statistical model structures and (ii) dynamically and statistically downscaled climate models. We sample the climate models by analyzing projections from the North American Coordinated Regional Downscaling Experiment (NA-CORDEX) dataset⁴² and the Multivariate Adaptive Constructed Analogs (MACAv2-METDATA) dataset⁴³.

Our projections sample different climate model structures, model resolutions, and downscaling methods. These differences lead to sizeable variation in the extreme rainfall projections (Figs. 3b, d, f). Choosing just a subset of the considered climate projections can drastically undersample the apparent deep uncertainties.

The reliability of stormwater infrastructure designs can be highly sensitive to the considered deep uncertainties (Fig. 4). We quantify reliability for this stormwater drainage pipe design as the probability that it does not flood over the specified lifetime⁴⁴. The projected reliabilities are deeply uncertain, as they are impacted by deep uncertainty projections of rainfall, surface runoff characteristics and infrastructure lifetime. The key driver of this uncertainty surrounding hydraulic reliability is the deep uncertainty surrounding extreme rainfall projections (Supplemental Table S4). Designing infrastructure in the face of deep and dynamic uncertainties poses, of course, highly complex decision problems^{9,22,45,46}. Using the simple and salient example of designing a stormwater drainage pipe, we demonstrate that climate uncertainty is the dominant driver of the decision-relevant metric of hydraulic reliability.

We show how increasing investments can increase reliability and robustness against deep uncertainty. In our simple examples, adding safety factors of 1.4 to 1.7 to the pipe diameter from the standard design guidance roughly achieves the 1/100-year hydraulic reliability in a way that is robust against the considered deep uncertainties in all three considered locations (Fig. 4). Safety factors of 2.0 to 2.3 can achieve the 1/500-year hydraulic reliability (Fig. 4). This is, of course, just a hypothetical case for selected locations in the U.S.A. Expanding this simple analysis to inform the design of workable and acceptable design guidance poses nontrivial research questions at the interface between disciplines such as Earth sciences, engineering, economics, ethics, political science, and law.

METHODS

Dataset description

We use the historical rainfall and temperature station observation from the United States National Oceanic and Atmospheric Administration (NOAA) National Center for Environmental Information data portal (<https://www.ncdc.noaa.gov/>).

We consider potential physical drivers of extreme rainfall as covariates for describing changes in statistics of extremes. Specifically, we use the historical winter mean (JFM) North Atlantic oscillation (NAO) index³¹ as a covariate for the nonstationary GEV model described below. For the Atlantic hurricane covariate time series, we use the number of Atlantic tropical cyclones from the United States National Oceanic and Atmospheric Administration (NOAA) Atlantic Oceanographic and Meteorological Laboratory data portal (<https://www.aoml.noaa.gov/hrd/tcfaq/E11.html>).

For the historical temperature time series, we use the daily air temperature record²⁸ from a station at the Baltimore/Washington International Thurgood Marshall Airport (BWI), Maryland, USA. We adopt the annual global mean surface air temperature dataset from the NOAA National Centers for Environmental Information data portal (<https://www.ncdc.noaa.gov/>). We use the Atlantic main development region (MDR) sea surface temperature from the National Centers for Environmental Information data portal (<https://www.ncdc.noaa.gov/>), and as projection we use the coupled model intercomparison project phase 5 (CMIP5) Global climate model (GCM)⁴⁷, namely, GFDL-ESM2M under Representative Concentration Pathway 8.5 (RCP8.5). We caution that our analysis does not account for internal variability, as well as model structural or parametric uncertainty regarding future projections of selected covariates. An assessment of the impacts of these uncertainties on projected extreme rainfall is another important avenue for future study.

We use sea surface temperature anomalies in the NINO3.4 region (averaged over 5⁰N-5⁰S, 120⁰W-170⁰W)³⁷ available on the NOAA National Centers for Environmental Information data portal (<https://www.ncdc.noaa.gov/teleconnections/enso/indicators/sst/>), and as projection we use the coupled model intercomparison project phase 5 (CMIP5) Global climate model (GCM), namely, GFDL-ESM2M under Representative Concentration Pathway 8.5 (RCP8.5). This region provides a good measure of important changes in sea surface temperature and its gradients that result in changes in the pattern of deep tropical convection and atmospheric circulation.

We use the Pacific decadal oscillation (PDO) index³⁶ and Southern oscillation index (SOI)³⁰ available on the NOAA National Weather Service Climate Prediction Center data portal (<https://www.cpc.ncep.noaa.gov/data/teledoc/telecontents.shtml>). The SOI is a measure of the large-scale fluctuations in air pressure occurring between the western and eastern tropical Pacific.

We incorporate rainfall time series from the Multivariate Adaptive Constructed Analogs (MACA) dataset⁴³. The MACAv2-METDATA dataset is the statistically downscaled subset of the coupled model intercomparison project phase 5 (CMIP5) Global climate models (GCMs). The MACA outputs include CCSM4, CanESM2, GFDL-ESM2M, Inmcm4, MIROC5, and MIROC-ESM.

We adopt rainfall time series from the North American Coordinated Regional Downscaling Experiment (NA-CORDEX) project available at 25-km resolution⁴². The NA-CORDEX dataset is the dynamically downscaled dataset. The NA-CORDEX dataset corresponds to a collection of high-resolution projections from different GCM-Regional climate model (RCM) combinations. The NA-CORDEX outputs include RegCM4 driven by MPI-ESM-LR, WRF driven by MPI-ESM-LR, and WRF driven by GFDL-ESM2M under Representative Concentration Pathway 8.5 (RCP8.5). We employ the non-parametric quantile mapping approach, called Kernel Density Distribution Mapping⁴⁸, to bias-correct the time series to match observations²¹. We select these

datasets for this proof-of-concept because they all are publicly available, frequently used for climate change impact assessments, and often used to inform flood-sensitive infrastructure design^{20,21,49}. We caution that our analysis relies on selected GCMs and thus likely undersamples the full range of relevant uncertainties. Future work might consider incorporating additional GCMs.

Extreme value model

We model the extreme rainfall using a nonstationary Generalized Extreme Value (GEV) distribution. The GEV permits accounting for the potential nonstationarity in annual flood peaks by specifying time-dependent model parameters. The GEV distribution includes the location (μ), scale (σ), and shape parameter (ξ) to specify the center, spread, and tail behavior, respectively. The probability density function of the GEV distribution is:

$$f(x) = \begin{cases} \frac{1}{\sigma} \left(1 + \xi \frac{x - \mu}{\sigma}\right)^{-1 - \frac{1}{\xi}} e^{-\left(1 + \xi \frac{x - \mu}{\sigma}\right)^{-\frac{1}{\xi}}}, & \text{for } 1 + \xi \frac{x - \mu}{\sigma} > 0 \\ \frac{1}{\sigma} e^{\frac{\mu - x}{\sigma}} e^{-\frac{\mu - x}{\sigma}}, & \text{for } \xi = 0 \\ 0, & \text{otherwise} \end{cases} \quad (1)$$

The GEV distribution is a flexible distribution that allows for heavy and light tails. Based on the shape parameter, the GEV can take one of three forms: i) Frechet, or lower bounded with a heavy upper-tailed, if ξ is positive; ii) Gumbel, or unbounded with heavy upper tails, if ξ is zero; iii) "Reverse" Weibull, or upper bounded with heavy lower tails, if ξ is negative⁵⁰.

We incorporate potential nonstationarity into the GEV model by allowing the location parameter (μ) to covary with different physical processes (T)³⁴:

$$\mu = \mu_0 (1 + a_\mu T), \quad (2)$$

where T is the covariate, μ_0 is the location parameter when $T=0$, and a_μ is the sensitivity of location parameter with respect to changes in the covariate.

We integrate a Bayesian-based Markov chain Monte Carlo approach into the nonstationary GEV for uncertainty assessment. We use a Bayesian approach to fit the nonstationary GEV distributions to the annual maximum rainfall intensity. Bayes' theorem combines the prior knowledge regarding the model parameters with the information gained from the observational data (i.e., the likelihood function) into the posterior distribution of the model parameters, given the data ($p(\theta|x)$):

$$p(\theta|x) \propto L(\theta)p(\theta), \quad (3)$$

where $L(\theta)$ is the likelihood function and $p(\theta)$ is the prior distribution of random variable θ . Our objective is to approximate the posterior distribution ($p(\theta|x)$) by drawing samples via Markov chain Monte Carlo (MCMC). For a random $X = \{x_1, x_2, \dots, x_n\}$, the likelihood function $L(\theta)$ for the parameter vector θ associated with its PDF $f_x(x)$ is defined as:

$$L(\theta) = \prod_{i=1}^n f_x(x_i|\theta). \quad (4)$$

We use a Gaussian prior distribution centered at 0, with a wide variance $N(0,100)$ for each model parameter. We sample from the posterior distribution ($p(\theta|x)$) of the model parameters using the Metropolis-Hastings algorithm⁵¹. We sample each GEV parameter successively for 50,000 iterations. The first 10,000 iterations are discarded for burn-in. We use the remaining 40,000 samples to serve as the ensemble for analysis. The best guess estimate refers to the parameter set with the highest posterior density value among all MCMC samples. To account for the uncertainty of rainfall intensity, we consider the full ensemble of parameter samples.

We construct a nonstationary GEV model that allows integrating relevant physical drivers of extreme rainfall as covariates. Incorporating physical-related covariates into the GEV distribution assists the statistical model to avoid unrealistic extrapolations.

Goodness-of-fit measures

We employ several metrics for model comparison. We compute two penalized-likelihood criteria- the Akaike information criterion³⁸ (AIC) and the Deviance information criterion³⁹ (DIC). The AIC and DIC penalize models based on their goodness-of-fit as well as the effective number of model parameters. For all three criteria, models with smaller values are typically preferred over those with larger values. The AIC is defined as

$$AIC = -2 \log(L_{max}) + 2N_p, \quad (5)$$

where, L_{max} is the maximum value of the likelihood function within the posterior model ensemble and N_p is the number of model parameters.

For a given model structure, the deviance for a given set of model parameters is given by

$$D(\theta) = -2 \log(L(\theta)). \quad (6)$$

We denote the expected value of $D(\theta)$ over θ as \bar{D} , and $\bar{\theta}$ as the expected value of θ . The effective number of parameters is calculated as $P_D = \bar{D} - D(\bar{\theta})$. The DIC is then defined as

$$DIC = P_D + \bar{D}. \quad (7)$$

Reliability assessment

We assess the reliability of hydraulic performance of stormwater drainage pipe. From reliability theory⁵², a limit state function (G) is defined as

$$G(q) = Q_p - Q_y, \quad (8)$$

where, q is the random variable that represents, for example, the pipe's flow in our study, Q_p is the pipe's flow capacity and Q_y is the flow load. The failure probability (P_f) can be expressed as

$$P_f = \text{probability} [G(q) < 0]. \quad (9)$$

Hydraulic reliability (R) of a stormwater pipe design is defined as

$$R = 1 - P_f. \quad (10)$$

The flow load and the pipe's flow capacity in a hydraulic design of stormwater pipes are defined using a criterion that the peak flow is not larger than the flow capacity of pipes. We use the peak flow from the rational method⁵³ to estimate flow load:

$$Q_y = 0.278CIA, \quad (11)$$

where, Q_y is the flow load (m^3/s), C is the runoff coefficient (dimensionless), I is rainfall intensity (mm/hr), and A is the contributing drainage area (km^2). The runoff coefficient represents the interaction of many complex factors, including infiltration, antecedent moisture, land cover, ground slopes, and soil types. It indicates the amount of runoff generated given an average intensity of rainfall for a storm.

We design the stormwater pipes for open-channel flow. We use the Manning's equation⁵³ to estimate the flow capacity of a circular pipe running full, but not under pressure:

$$Q_p = \frac{0.31}{n} D^{8/3} S^{1/2}, \quad (12)$$

where, n is the Manning's roughness coefficient representing the resistance to flows in pipe, D is the pipe diameter (m), and S is the pipe bottom slope. We consider a concrete pipe with Manning's roughness, $n = 0.013$, and a contributing drainage area of 0.25 km^2 .

Uncertainty decomposition

We employ the cumulative uncertainty approach⁵⁴ to assess the influential uncertainty sources in the hydraulic reliability of stormwater pipe design. The approach decomposes the total uncertainty to individual uncertainty sources, such that the sum of the uncertainties from individual sources is always equal to the total uncertainty in the reliability of the pipe. We consider uncertainty from three key sources: climate, surface runoff characteristics, and service life of the pipe. We quantify both the individual and combined sources of uncertainty. We consider nine sets

of climate model outputs, four sets of surface runoff characteristics and three sets of pipe service life (Supplemental Table S3). This produces a total of 108 scenarios.

We assess the uncertainty contribution from each source (climate, surface runoff characteristics, and service life of the pipe), called here as stage uncertainty. Stage uncertainty is the sum of the variation of the main effect of stage k and the variations of the interactions between stage k and stages after k . To quantify the uncertainty contribution from each stage, we first compute the conditional cumulative uncertainty up to a particular stage. Conditional cumulative uncertainty up to a particular stage represents the variation in the reliability due to the design choices up to that stage, while the choices beyond that stage are fixed. Then the marginal cumulative uncertainty up to a particular stage is an average of conditional cumulative uncertainties. We compute the uncertainty of each stage as the difference between successive marginal cumulative uncertainties.

We denote the total number of stages in the reliability estimates by K , where in this case $K=3$, i.e., climate, surface runoff characteristics, and service life of the pipe. For a particular stage k , there are n_k models/scenarios denoted by χ_k . The cumulative uncertainty up to stage k is defined as the variation in the reliability due to the choice of models/scenarios up to stage k , while the models/scenarios after stage k are fixed. The cumulative uncertainty up to stage k is denoted by $U^{cum}(\chi_1, \dots, \chi_k)$. For a specific model/scenario, of stage k for $k=1, \dots, K$, we let $P(x_1, x_2, \dots, x_K)$ be the reliability of stormwater drainage design using the models/scenarios $x_k, k = 1, \dots, K$. For a given model/scenario, after stage k , the set of reliabilities are:

$$q_{x_{k+1}, \dots, x_K} = \{P(x_1, \dots, x_k, x_{k+1}, \dots, x_K) : x_j \in \chi_j, j = 1, \dots, k\}. \quad (13)$$

Then $U^{cum}(q_{x_{k+1}, \dots, x_K})$ can be interpreted as the conditional cumulative uncertainty up to stage k while the models/scenarios after stage k are fixed as x_{k+1}, \dots, x_K . The marginal cumulative uncertainty up to stage k is the average of conditional cumulative uncertainties defined as:

$$U^{cum}(\chi_1, \dots, \chi_k) = \frac{1}{\prod_{j=k+1}^K n_j} \sum_{x_{k+1} \in \chi_{k+1}} \dots \sum_{x_K \in \chi_K} U(q_{x_{k+1}, \dots, x_K}). \quad (14)$$

Since the cumulative uncertainty is monotonously increasing⁵⁴, we can define the uncertainty of each stage as the difference between successive cumulative uncertainties. That is, the uncertainty of stage k , denoted by $U^{cum}(\chi_k)$, can be defined as:

$$U^{cum}(\chi_k) = U^{cum}(\chi_1, \dots, \chi_k) - U^{cum}(\chi_1, \dots, \chi_{k-1}). \quad (15)$$

The uncertainty of each stage is the amount of contribution to the cumulative uncertainty.

Also, the sum of uncertainties of individual stages is always equal to the total uncertainty

$U^{cum}(\chi_1, \dots, \chi_k)$. We express both the stage and cumulative uncertainties in terms of the variance⁵⁵ in the reliability of stormwater pipe design. Let, $y = q_{x_{k+1}, \dots, x_K}$ and a set of $y = \{y_1, \dots, y_n\}$. The variance is defined as:

$$\text{Variance} = \frac{1}{n} \sum_{i=1}^n (y_i - \bar{y})^2, \quad (16)$$

where, $\bar{y} = \frac{1}{n} \sum_{i=1}^n y_i$.

The cumulative uncertainty approach has several advantages over the commonly used analysis of variance (ANOVA) framework. The ANOVA approach partitions the total variance into components attributed to the individual sources and the components attributed to interaction⁵⁵. The ANOVA approach has several key limitations⁵⁴: (1) sensitive to outliers; (2) assumes the projections are normally distributed; (3) model selection is challenging; and (4) difficult to characterize how interaction effects drive uncertainty in projections. The cumulative uncertainty approach allows us to quantify the relative contribution of each stage to the total uncertainty in the reliability estimates and to identify how uncertainties are propagated as the stages proceed in the stormwater pipe design.

Acknowledgements

This work was co-supported by the National Oceanic and Atmospheric Administration (NOAA) through the Mid-Atlantic Regional Integrated Sciences and Assessments (MARISA) program under NOAA grant NA16OAR4310179 and by the Penn State Center for Climate Risk Management. All errors and opinions are from the authors and do not reflect the funding agencies. We thank Amir AghaKouchak for helpful comments on a previous draft. We thank Lauren Cook, Costantine Samaras, and Seth McGinnis for sharing the North American Coordinated Regional Downscaling Experiment (NA-CORDEX) dataset. We are grateful to Irene Schaperdoth, Tony Wong, Murali Haran, and Skip Wishbone for valuable inputs.

Disclaimer and License

The results, data, software tools, and other resources related to this work are provided under the GNU general public open-source license, as-is, without warranty of any kind, expressed or implied. In no event shall the authors or copyright holders be liable for any claim, damages or other liability in connection with the use of these resources. This is academic research and not designed to be used to guide a specific decision.

Author contributions

All authors contributed to the study design. S.S. and B.L. constructed the nonstationary statistical model. S.S. led the calculations. S.S. and K.K wrote the initial draft of the manuscript. All authors revised and edited the manuscript.

Data and Code Availability

The code used for this analysis and the data required to plot the results is available at Github repository <https://github.com/svs6308/PipeDesign>.

Competing interests

The authors are not aware of any competing financial or nonfinancial interests.

Materials & Correspondence

Correspondence and requests for materials should be addressed to the corresponding author at sanjibsharma66@gmail.com

References

1. Intergovernmental Panel on Climate Change. *Managing the Risks of Extreme Events and Disasters to Advance Climate Change Adaptation: Special Report of the Intergovernmental Panel on Climate Change*. (Cambridge University Press, 2012).
2. Desai, B., Maskrey, A., Peduzzi, P., De Bono, A. & Herold, C. Making development sustainable: the future of disaster risk management, global assessment report on disaster risk reduction. (2015).
3. Winsemius, H. C. *et al.* Global drivers of future river flood risk. *Nat. Clim. Chang.* **6**, 381–385 (2015).
4. Hirabayashi, Y. *et al.* Global flood risk under climate change. *Nat. Clim. Chang.* **3**, 816–821 (2013).
5. Jongman, B. Effective adaptation to rising flood risk. *Nat. Commun.* **9**, 1986 (2018).
6. Wong, T. E. & Keller, K. Deep Uncertainty Surrounding Coastal Flood Risk Projections: A Case Study for New Orleans. *Earth's Future* vol. 5 1015–1026 (2017).
7. Brown, S. A. *et al.* *Urban drainage design manual: hydraulic engineering circular 22*. <https://rosap.nrl.bts.gov/view/dot/44353> (2009).
8. Schueler, T. R. & Claytor, R. A. Maryland stormwater design manual volumes I and II. *Center for Watershed Protection and Maryland Dep. of the Environment, Baltimore, Md* (2000).

9. Lopez-Cantu, T. & Samaras, C. Temporal and spatial evaluation of stormwater engineering standards reveals risks and priorities across the United States. *Environ. Res. Lett.* **13**, 074006 (2018).
10. Cheng, L. & AghaKouchak, A. Nonstationary Precipitation Intensity-Duration-Frequency Curves for Infrastructure Design in a Changing Climate. *Scientific Reports* vol. 4 (2015).
11. Wright, D. B., Bosma, C. D. & Lopez-Cantu, T. US hydrologic design standards insufficient due to large increases in frequency of rainfall extremes. *Geophys. Res. Lett.* **46**, 8144–8153 (2019).
12. Bonnin, G. M. *et al.* Precipitation-frequency atlas of the United States: NOAA Atlas 14, volume 1, version 4. *NOAA, National Weather Service, Silver Spring, Maryland* (2006).
13. Allan, R. P. & Soden, B. J. Atmospheric warming and the amplification of precipitation extremes. *Science* **321**, 1481–1484 (2008).
14. Protecting Public Health and the Environment and Restoring Science To Tackle the Climate Crisis. *Presidential Documents* <https://www.govinfo.gov/content/pkg/FR-2021-01-25/pdf/2021-01765.pdf> (2021).
15. Salas, J. D., Obeysekera, J. & Vogel, R. M. Techniques for assessing water infrastructure for nonstationary extreme events: a review. *Hydrol. Sci. J.* **63**, 325–352 (2018).
16. Woldemeskel, F. M., Sharma, A., Sivakumar, B. & Mehrotra, R. Quantification of precipitation and temperature uncertainties simulated by CMIP3 and CMIP5 models. *J. Geophys. Res. D: Atmos.* **121**, 3–17 (2016).
17. Lempert, R. J. A new decision sciences for complex systems. *Proc. Natl. Acad. Sci. U. S. A.* **99 Suppl 3**, 7309–7313 (2002).
18. Lempert, R. J. & Collins, M. T. Managing the risk of uncertain threshold responses: comparison of robust, optimum, and precautionary approaches. *Risk Anal.* **27**, 1009–1026 (2007).
19. Stehfest, E. *et al.* Key determinants of global land-use projections. *Nat. Commun.* **10**, 2166 (2019).
20. Mallakpour, I., AghaKouchak, A. & Sadegh, M. Climate-Induced Changes in the Risk of Hydrological Failure of Major Dams in California. *Geophys. Res. Lett.* **46**, 2130–2139 (2019).
21. Cook, L. M., McGinnis, S. & Samaras, C. The effect of modeling choices on updating intensity-

- duration-frequency curves and stormwater infrastructure designs for climate change. *Clim. Change* **159**, 289–308 (2020).
22. Chester, M. V., Shane Underwood, B. & Samaras, C. Keeping infrastructure reliable under climate uncertainty. *Nature Climate Change* (2020) doi:10.1038/s41558-020-0741-0.
 23. Manocha, N. & Babovic, V. Sequencing Infrastructure Investments under Deep Uncertainty Using Real Options Analysis. *Water* vol. 10 229 (2018).
 24. Smith, A. B. 2017 US billion-dollar weather and climate disasters: a historic year in context. *Report From Climate. gov*, <https://www.climate.gov/news-features/blogs/beyond-data/2017-us-billion-dollar-weather-and-climate-disasters-historic-year>, Accessed June 28, 2019 (2018).
 25. Viterbo, F. *et al.* A Multiscale, Hydrometeorological Forecast Evaluation of National Water Model Forecasts of the May 2018 Ellicott City, Maryland, Flood. *J. Hydrometeorol.* **21**, 475–499 (2020).
 26. Eden, J. M., Wolter, K. & Otto, F. E. L. Multi-method attribution analysis of extreme precipitation in Boulder, Colorado. *Environmentalist* (2016).
 27. Vahedifard, F., AghaKouchak, A., Ragno, E., Shahrokhbabadi, S. & Mallakpour, I. Lessons from the Oroville dam. *Science* vol. 355 1139.2–1140 (2017).
 28. DeGaetano, A. T., Noon, W. & Eggleston, K. L. Efficient Access to Climate Products using ACIS Web Services. *Bulletin of the American Meteorological Society* vol. 96 173–180 (2015).
 29. Zarekarizi, M., Srikrishnan, V. & Keller, K. Neglecting uncertainties biases house-elevation decisions to manage riverine flood risks. *Nat. Commun.* **11**, 5361 (2020).
 30. Ropelewski, C. F. & Jones, P. D. An extension of the Tahiti–Darwin southern oscillation index. *Mon. Weather Rev.* **115**, 2161–2165 (1987).
 31. Jones, P. D., Jónsson, T. & Wheeler, D. Extension to the North Atlantic Oscillation using early instrumental pressure observations from Gibraltar and south-west Iceland. *International Journal of Climatology: A Journal of the Royal Meteorological Society* **17**, 1433–1450 (1997).
 32. Lapp, S. L., St. Jacques, J.-M., Barrow, E. M. & Sauchyn, D. J. GCM projections for the Pacific Decadal Oscillation under greenhouse forcing for the early 21st century. *Int. J. Climatol.* **32**, 1423–

- 1442 (2012).
33. Wong, T. E., Klufas, A., Srikrishnan, V. & Keller, K. Neglecting model structural uncertainty underestimates upper tails of flood hazard. *Environmental Research Letters* vol. 13 074019 (2018).
 34. Ragno, E., AghaKouchak, A., Cheng, L. & Sadegh, M. A generalized framework for process-informed nonstationary extreme value analysis. *Adv. Water Resour.* **130**, 270–282 (2019).
 35. Grinsted, A., Moore, J. C. & Jevrejeva, S. Projected Atlantic hurricane surge threat from rising temperatures. *Proc. Natl. Acad. Sci. U. S. A.* **110**, 5369–5373 (2013).
 36. Mantua, N. J., Hare, S. R., Zhang, Y., Wallace, J. M. & Francis, R. C. A Pacific Interdecadal Climate Oscillation with Impacts on Salmon Production. *Bulletin of the American Meteorological Society* vol. 78 1069–1079 (1997).
 37. Reynolds, R. W., Rayner, N. A., Smith, T. M., Stokes, D. C. & Wang, W. An Improved In Situ and Satellite SST Analysis for Climate. *Journal of Climate* vol. 15 1609–1625 (2002).
 38. Akaike, H. A new look at the statistical model identification. *IEEE Trans. Automat. Contr.* **19**, 716–723 (1974).
 39. Spiegelhalter, D. J., Best, N. G., Carlin, B. P. & van der Linde, A. Bayesian measures of model complexity and fit. *Journal of the Royal Statistical Society: Series B (Statistical Methodology)* vol. 64 583–639 (2002).
 40. Wise, E. K., Wrzesien, M. L., Dannenberg, M. P. & McGinnis, D. L. Cool-Season Precipitation Patterns Associated with Teleconnection Interactions in the United States. *Journal of Applied Meteorology and Climatology* vol. 54 494–505 (2015).
 41. Hoell, A. *et al.* Does El Niño intensity matter for California precipitation? *Geophysical Research Letters* vol. 43 819–825 (2016).
 42. Mearns, L. O. *et al.* The NA-CORDEX dataset, version 1.0. *NCAR Climate Data Gateway. Boulder (CO): The North American CORDEX Program* **10**, D6SJ1JCH (2017).
 43. Abatzoglou, J. T. & Brown, T. J. A comparison of statistical downscaling methods suited for wildfire applications. *Int. J. Climatol.* **32**, 772–780 (2012).

44. Tran Huu D. Markov-Based Reliability Assessment for Hydraulic Design of Concrete Stormwater Pipes. *J. Hydraul. Eng.* **142**, 06016005 (2016).
45. Herman, J. D., Reed, P. M., Zeff, H. B. & Characklis, G. W. How should robustness be defined for water systems planning under change? *Journal of Water Resources Planning and Management* **141**, 04015012 (2015).
46. Bryant, B. P. & Lempert, R. J. Thinking inside the box: A participatory, computer-assisted approach to scenario discovery. *Technol. Forecast. Soc. Change* **77**, 34–49 (2010).
47. Taylor, K. E., Stouffer, R. J. & Meehl, G. A. An Overview of CMIP5 and the Experiment Design. *Bull. Am. Meteorol. Soc.* **93**, 485–498 (2012).
48. McGinnis, S., Nychka, D. & Mearns, L. O. A New Distribution Mapping Technique for Climate Model Bias Correction. *Machine Learning and Data Mining Approaches to Climate Science* 91–99 (2015) doi:10.1007/978-3-319-17220-0_9.
49. Lopez-Cantu, T., Prein, A. F. & Samaras, C. Uncertainties in Future U.S. Extreme Precipitation From Downscaled Climate Projections. *Geophys. Res. Lett.* **47**, WO3410 (2020).
50. Coles, S. *An Introduction to Statistical Modeling of Extreme Values*. (Springer, London, 2001).
51. Chib, S. & Greenberg, E. Understanding the Metropolis-Hastings Algorithm. *The American Statistician* vol. 49 327–335 (1995).
52. Melchers, R. E. & Beck, A. T. *Structural Reliability Analysis and Prediction*. (John Wiley & Sons, 2018).
53. Mays, L. W. *Water Resources Engineering*. (John Wiley & Sons, 2010).
54. Kim, Y., Ohn, I., Lee, J.-K. & Kim, Y.-O. Generalizing uncertainty decomposition theory in climate change impact assessments. *Journal of Hydrology X* **3**, 100024 (2019).
55. Bosshard, T. *et al.* Quantifying uncertainty sources in an ensemble of hydrological climate-impact projections. *Water Resour. Res.* **49**, 1523–1536 (2013).
56. Lempert, R. J., Groves, D. G., Popper, S. W. & Bankes, S. C. A General, Analytic Method for Generating Robust Strategies and Narrative Scenarios. *Manage. Sci.* **52**, 514–528 (2006).

57. Atlas, N. *Precipitation-Frequency Atlas of the United States*. (14AD).
58. Heaney, J. P., Sample, D. & Wright, L. *Costs of Urban Stormwater Control*. (U.S. Environmental Protection Agency, Office of Research and Development, National Risk Management Research Laboratory, 2002).
59. Randall, F. A. The safety factor of structures in history. *Prof. Saf.* 12–28 (1976).
60. Kass, R. E. & Raftery, A. E. Bayes Factors. *J. Am. Stat. Assoc.* **90**, 773–795 (1995).

Figures:

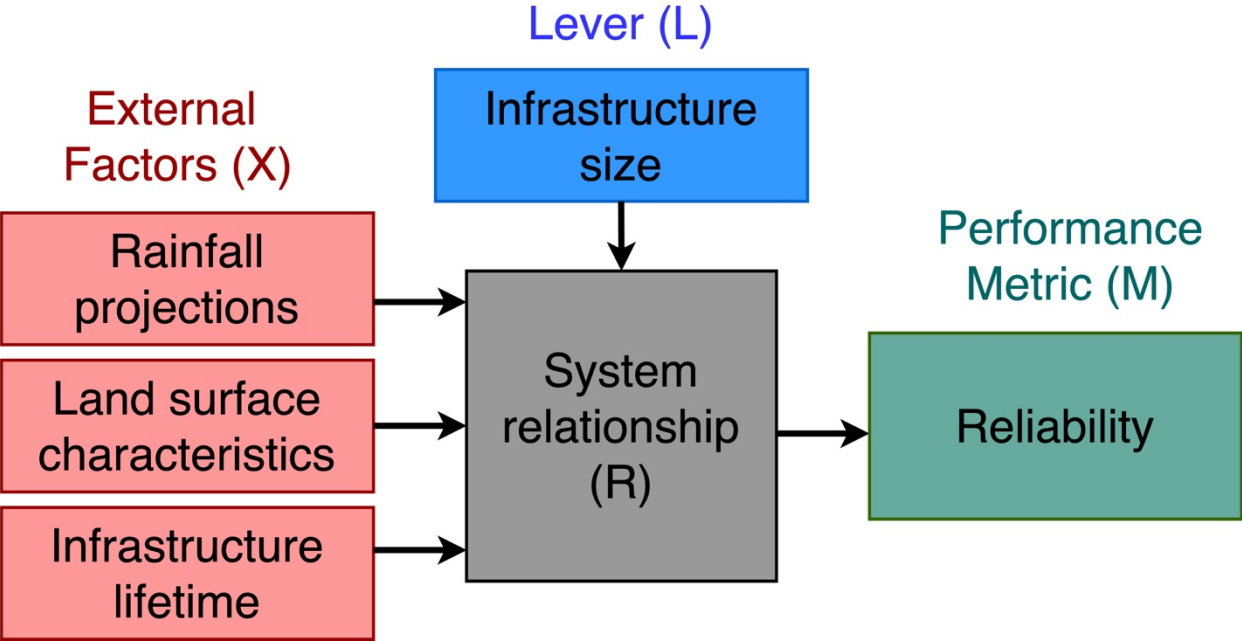


Fig. 1: Flow diagram for the decision-analysis. The XLRM framework⁵⁶ illustrates the relationship between the external factors (X), levers the decision-maker can manipulate to affect the outcome (L), the modeling relationship (R) and the performance metric (M).

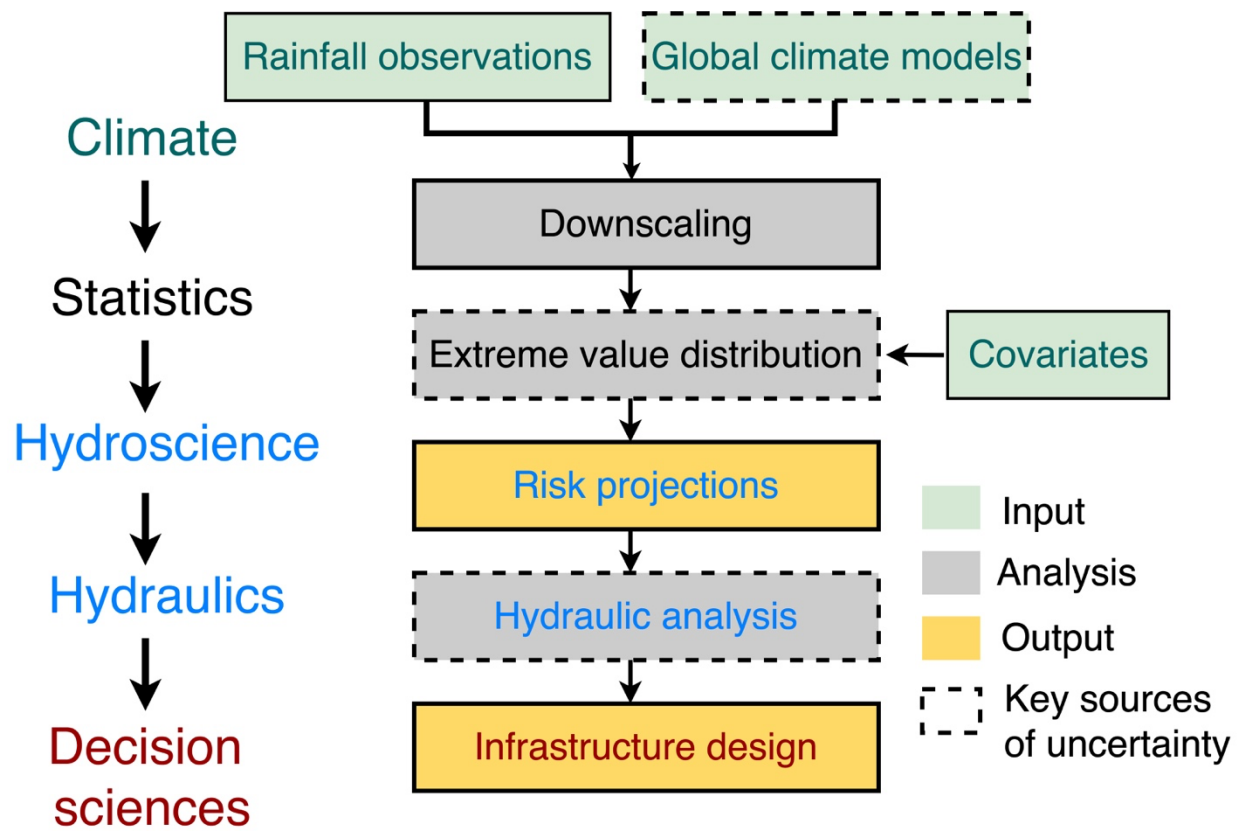


Fig. 2: Diagrammatic representation of the design analysis for stormwater drainage size.

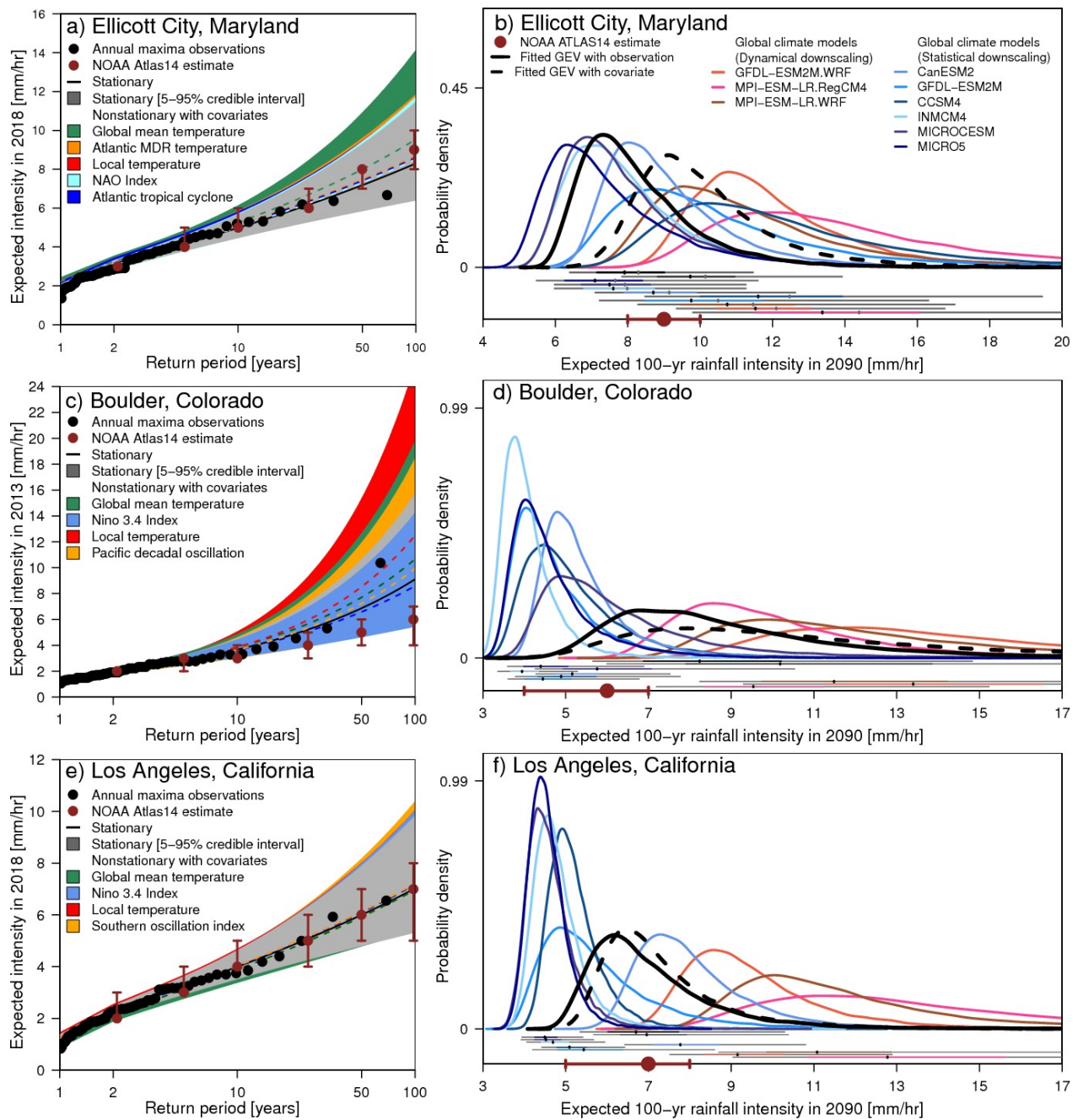
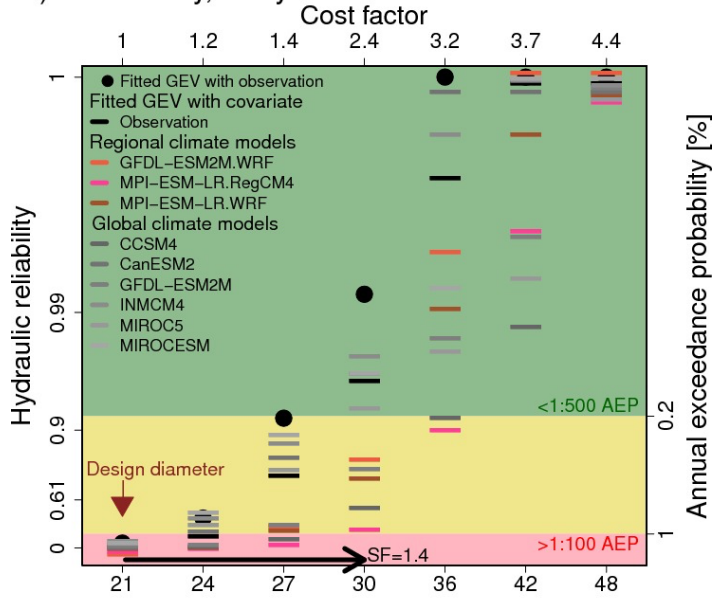


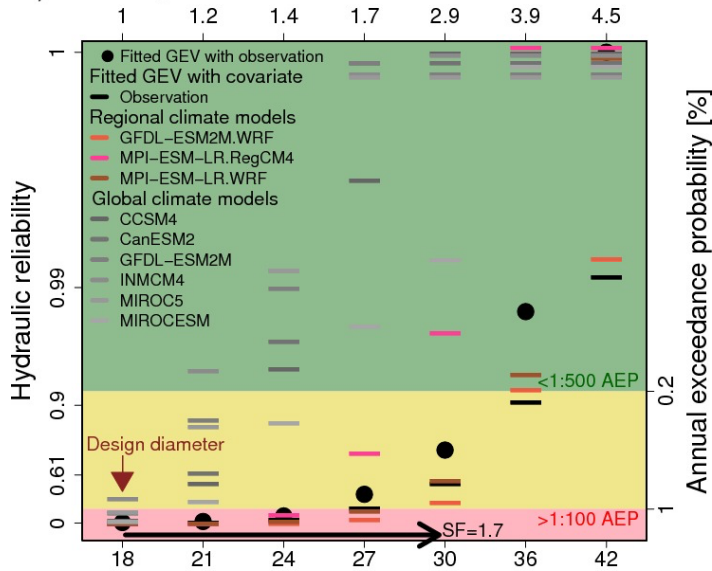
Fig. 3: Expected current and future rainfall return periods. **a**, Expected rainfall intensity in Ellicott City, Maryland in 2018 for different return periods under the stationary and nonstationary assumptions. The dotted lines are the expected return levels and the corresponding color bound shows the 5%-95% credible interval. The brown dots represent the United States National Oceanic and Atmospheric Administration (NOAA) Atlas 14 estimates⁵⁷; and the corresponding error bars represent the 90% confidence bound. We compute nonstationary rainfall intensity using Generalized

Extreme Value (GEV) distribution fitted with different covariates. Selected covariates are global mean temperature, Atlantic Main Development Region (MDR) temperature, local temperature, North Atlantic Oscillation (NAO) index and number of Atlantic tropical cyclones. We calculate the Akaike Information Criterion (AIC) and Deviance Information Criterion (DIC) to assess the goodness-of-fit for GEV distribution. For the observed rainfall intensity, the selected metrics choose the GEV distribution with MDR temperature as the best nonstationary model. **b**, Projected daily rainfall intensity in 2090 using GEV distribution fitted with historical observation (1951-2018) and climate model outputs (2020-2090) using MDR temperature as a covariate. We use the North American Coordinated Regional Downscaling Experiment (NA-CORDEX)⁴² project dataset, which are dynamically downscaled products. The Multivariate Adaptive Constructed Analogs (MACA)⁴³ data sets are statistically downscaled subset of the coupled model intercomparison project phase 5 (CMIP5) Global climate models (GCMs). **c**, Expected rainfall intensity in Boulder, Colorado in 2013 for different return periods under the stationary and nonstationary assumptions. Selected covariates are local temperature than the global mean surface temperature, the Pacific decadal oscillation index and the Nino 3.4 index. For the observed rainfall intensity, the selected metrics choose the GEV distribution with local temperature as the best nonstationary model. **d**, Projected daily rainfall intensity in 2090 using GEV distribution fitted with historical observation (1951-2018) and climate model outputs (2020-2090) using local temperature as a covariate. **e**, Expected rainfall intensity in Los Angeles, California in 2018 for different return periods under the stationary and nonstationary assumptions. Selected covariates are global mean surface temperature, local temperature, the Nino 3.4 index and the Southern oscillation index. We choose the Nino 3.4 index as a covariate to project extreme rainfall intensity in Los Angeles. **f**, Projected daily rainfall intensity in 2090 using GEV distribution fitted with historical observation (1951-2018) and climate model outputs (2020-2090) using the Nino 3.4 index as a covariate.

a) Ellicott City, Maryland



b) Boulder, Colorado



c) Los Angeles, California

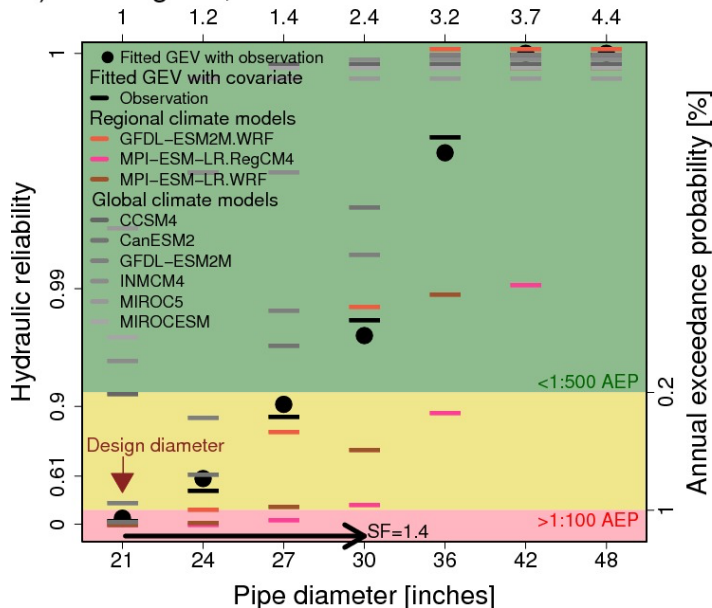


Fig. 4: Lifetime hydraulic reliability of stormwater drainage pipe. Lifetime hydraulic reliability of stormwater pipe conditioned on the deeply uncertain extreme rainfall projections, surface imperviousness and pipe lifetime. We assume a concrete pipe with Manning's roughness, $n=0.013$, and a contributing drainage area of 0.25 km^2 . Cost factors⁵⁸ (top x-axis) are relative to the design diameter. Design diameter is the resulting diameter with daily rainfall intensity from the United States National Oceanic and Atmospheric Administration (NOAA) ATLAS 14 estimates⁵⁷ for the selected stations: a) Baltimore/Washington International Thurgood Marshall Airport, Maryland, b) Boulder Municipal Airport, Colorado, and c) Los Angeles International Airport, California. Safety factor (SF)⁵⁹ is a multiplier in a stormwater pipe diameter obtained from the standard design guidance. Safety factor allows to achieve the intended hydraulic reliability that is robust to the considered deep uncertainty.

Supplemental Information

Neglecting uncertainty can lead to failing stormwater infrastructures

Sanjib Sharma^{1*}, Ben Seiyon Lee², Robert E. Nicholas^{1,3}, Klaus Keller^{1,4}

¹Earth and Environmental Systems Institute, The Pennsylvania State University, University Park, PA, USA

²Department of Statistics, The George Mason University, Fairfax, VA, USA

³Department of Meteorology and Atmospheric Science, The Pennsylvania State University, University Park, PA, USA

⁴Department of Geosciences, The Pennsylvania State University, University Park, PA, USA

*Corresponding author



Supplementary tables

Table S1: Selected stations for analysis and the average annual daily maximum rainfall.

Station name	State	Latitude	Longitude	Elevation (m)	Average annual daily maximum rainfall (mm)
Baltimore/Washington International Thurgood Marshall Airport	Maryland	39.17	76.66	42.28	78.54
Boulder Municipal Airport	Colorado	39.99	105.26	1613.27	54.35
Los Angeles International Airport	California	33.94	118.38	34.92	59.31

Table S2: Goodness-of-fit results for stationary and nonstationary GEV distributions the selected locations.

Baltimore/Washington International Thurgood Marshall Airport, Maryland						
Goodness-of-fit measures	Model structures					
	Stationary	Nonstationary with covariates				
		Global Temp	Local Temp	MDR Temp	NAO Index	Tropical Cyclone
ΔAIC	4.22	2.16	6.19	0	4.07	5.51
ΔDIC	5.06	3.15	49.2	0	8.33	5.33
Boulder Municipal Airport, Colorado						
Goodness-of-fit measures	Model structures					
	Stationary	Nonstationary with covariates				
		Global Temp	Local Temp	NINO 3.4 Index	PDO Index	
ΔAIC	4.97	3.2	0	5.60	3.63	
ΔDIC	8.80	7.98	0	8.35	5.48	
Los Angeles International Airport, California						
Goodness-of-fit measures	Model structures					
	Stationary	Nonstationary with covariates				
		Global Temp	Local Temp	NINO 3.4 Index	SOI Index	
ΔAIC	-0.5	0.2	1.14	0	0.99	
ΔDIC	0.4	-0.4	0.66	0	1.02	

 Model choice indicated by each metric
  There is substantial evidence to support the candidate model

We construct a nonstationary GEV model with different covariates. We calculate the Akaike information criterion (AIC), and Deviance information criterion (DIC). Green denotes the chosen model for each metric. Light red denotes a competing GEV model structure. Extreme rainfall distribution in Ellicott City reflects a greater contribution from the average sea surface temperature in the Atlantic main development region³⁵ than the global mean surface temperature, local surface temperature, the North Atlantic Oscillation index and the number of Atlantic tropical cyclones. The Atlantic main development region (10⁰N-20⁰N, 80⁰W-20⁰W) is monitored for potential

tropical system development regions during the course of a given Atlantic hurricane season. For the observed rainfall distribution in Boulder, local temperature emerges as the best covariate choice, followed by the global mean surface temperature, the Pacific Decadal Oscillation index³⁶, and the Nino 3.4 index. In the context of Los Angeles, we notice that differences of goodness-of-fit measures⁶⁰ do not show sufficient evidence to select a specific model structure and/or covariates (e.g., global mean surface temperature, local temperature, Nino 3.4 index and Southern oscillation index). We estimate extreme rainfall intensity in Los Angeles by taking advantage of the dependence relationship in the time series of the Nino 3.4 index and historical rainfall observations. Previous studies^{40,41} suggest that the Nino 3.4 average sea surface temperature anomalies in the area of tropical Pacific Ocean (5°S–5°N, 120°–170°W) has a substantial influence on precipitation in many parts of California.

Table S3: Uncertain factors sampled to construct scenarios.

Climate model output	Surface runoff characteristic	Service life of the pipe (years)
Three sets of RCMs: RegCM4 driven by MPI-ESM-LR, WRF driven by MPI-ESM-LR, and WRF driven by GFDLESM2M. Six sets of GCMs: CCSM4, CanESM2, GFDL-ESM2M, inmcm4, MIROC5, and MIROC-ESM.	Light residential area Moderate urbanization Heavy urbanization Fully urbanization	Fifty Sixty Seventy

We consider three different sources of uncertainties: climate, surface runoff characteristics and service life of the pipe. Climate uncertainty refers to the uncertainty in climate model outputs due to several factors, such as internal variability, model assumptions, spatial resolution and downscaling techniques. Surface runoff characteristics indicate the fraction of rainfall landing on the drainage area that becomes stormwater runoff. It depends on the interaction of many complex

factors, including infiltration, antecedent moisture, land cover, ground slopes, and soil types.

Service life uncertainty refers to the uncertainty in the lifespan of the pipe.

Table S4: Variance decomposition in the reliability estimates of stormwater drainage pipe.

Uncertainty sources	Cumulative uncertainty	Individual uncertainty
Climate	0.00647616	0.006476166 (82%)
Surface runoff characteristics	0.00652754	5.1428E-05 (1%)
Service life of pipe	0.00788786	0.001360262 (17%)

Total uncertainty in the reliability of stormwater drainage design is the contribution from each individual uncertainty source. We find that the climate uncertainty dominates the decomposition of variance in the reliability of stormwater drainage design. Climate uncertainty contributes more than the combined effect of surface runoff characteristics and service life of the pipe. After the climate uncertainty, service life of the pipe plays the most important role. Surface runoff characteristics contribute 17% of the total variance in the reliability of stormwater drainage design. We find that the surface runoff characteristics exhibit relatively small contributions compared to any other uncertainty source. Note that these contributions only represent relative influence but not absolute impacts. Therefore, the near-zero contribution of surface runoff characteristics does not specify there is no influence, but indicates the influence is relatively smaller than others.

Prior Distribution Sensitivity Test

We conduct a sensitivity test on the specification of prior distributions. We consider two generalized extreme value (GEV) distributions: stationary and non-stationary location parameter. GEV model is fit to the observed dataset with Atlantic Main Development Region (MDR) temperature as a covariate. We examine three sets of prior distributions for each GEV model. For the first set, we place a uniform prior distribution on each GEV model parameter. For the second

set, we use a Gaussian prior distribution with a wide variance ($N(0,100)$) for each parameter. For the third set, we use a Gaussian prior distribution with a small variance ($N(0,10)$) for each parameter. Results show that parameter estimates do not substantially deviate with the choice of different prior distributions.

Table S5: Sensitivity test results for the GEV distribution with a non-stationary location parameter. We fit the distribution to the observed data under three different prior distributions. We show the posterior distribution mean and the 95% credible interval range in parentheses. The results are for Baltimore/Washington International Thurgood Marshall Airport.

Parameter	Uniform	$N(0,100)$	$N(0,10)$
Location	2.679(2.442,2.917)	2.676 (2.439,2.920)	2.683(2.445, 2.926)
Scale	0.904(0.723,1.100)	0.899 (0.712,1.101)	0.905 (0.720, 1.111)
Shape	0.156(0,0.339)	0.153 (0, 0.326)	0.155(0, 0.332)

Supplementary Figures

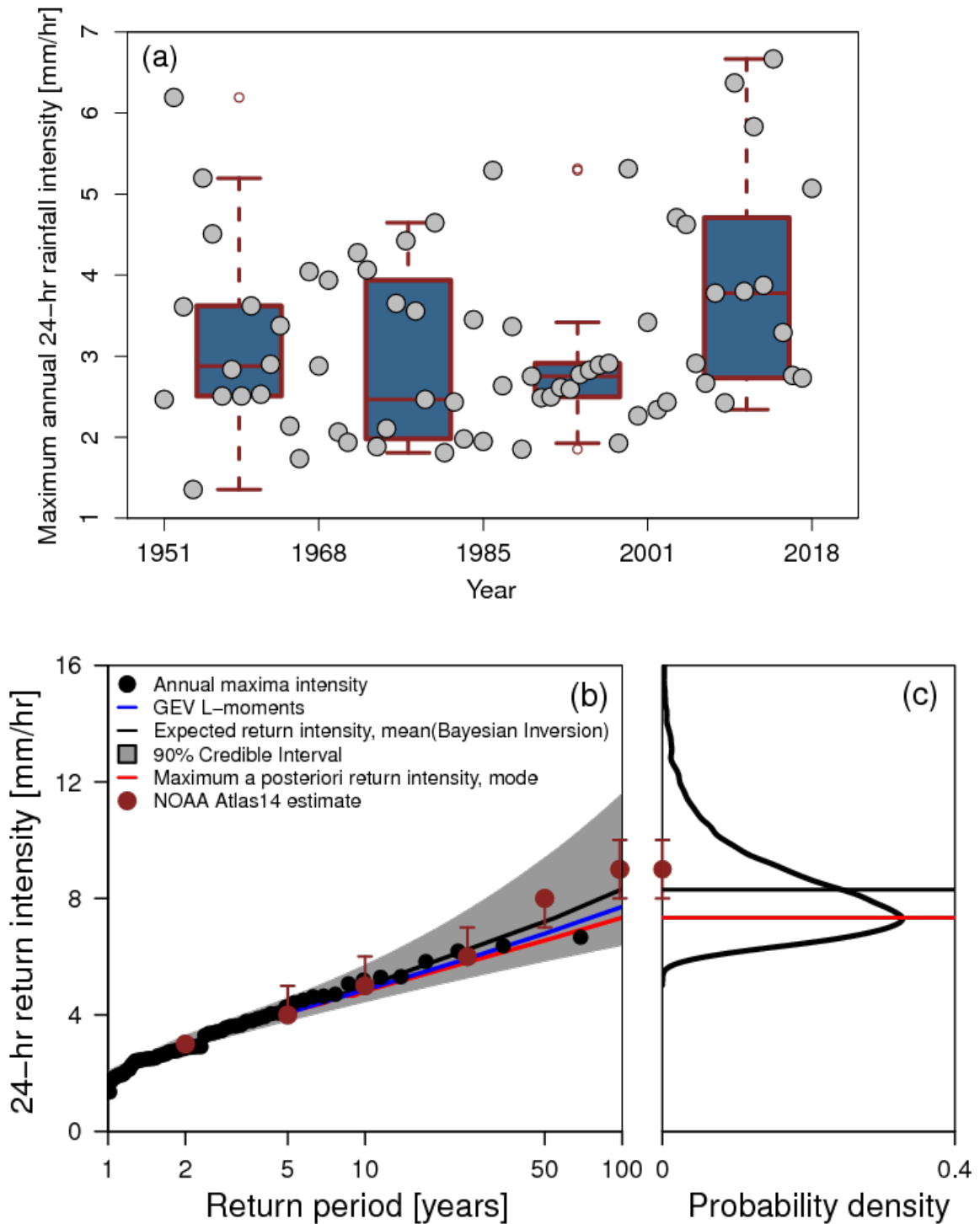


Figure S1: Changes in statistics of the daily rainfall maxima. **a**, Daily annual rainfall intensity²⁸ in Baltimore/Washington International Thurgood Marshall Airport (BWI), Maryland, USA. This is the closest rain gauge station to Ellicott City with a continuous rainfall record from

1951-2018. The box-and-whisker plots show the distribution of daily annual rainfall intensity maxima for the BWI station by binning the rainfall intensity into four blocks over the period of 1951–2018. The red circles indicate outliers. The black horizontal lines denote the median. **a**, 100-year storm comparison considering-uncertainty (black line and gray bounds) and ignoring-uncertainty (red line) under stationary assumption. We use Bayesian inference via Markov Chain Monte Carlo (MCMC) to calculate return period-return level curve and the corresponding 90% credible interval. We adopt the MCMC sample with the highest posterior probability samples as the best guess estimate of that parameter. To account for uncertainty in rainfall intensity, we consider the full ensemble of parameter samples. The red circles indicate the United States National Oceanic and Atmospheric Administration (NOAA) Atlas 14 estimates⁵⁷ for BWI station, and the corresponding bars represent the 90% confidence interval⁵⁷ (i.e., 5% and 95% confidence limits). **c**, Comparison of different estimates of the 100-yr intensity.

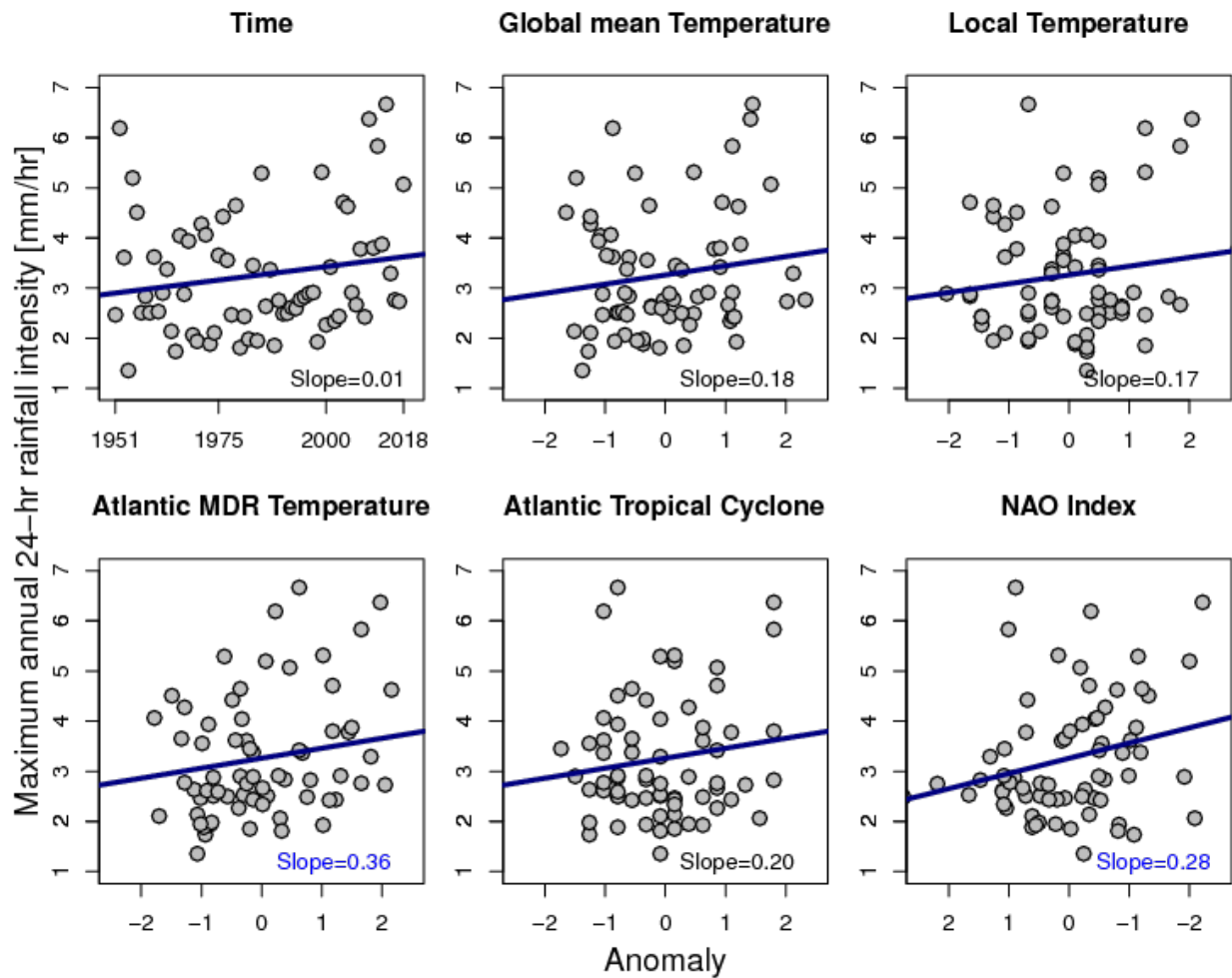


Figure S2: Maximum annual 24-hr rainfall intensity versus covariates for

Baltimore/Washington International Thurgood Marshall Airport. Blue line denotes the linear trend.

Blue font denotes that the 90 % confidence intervals for the upward slope do not include zero.

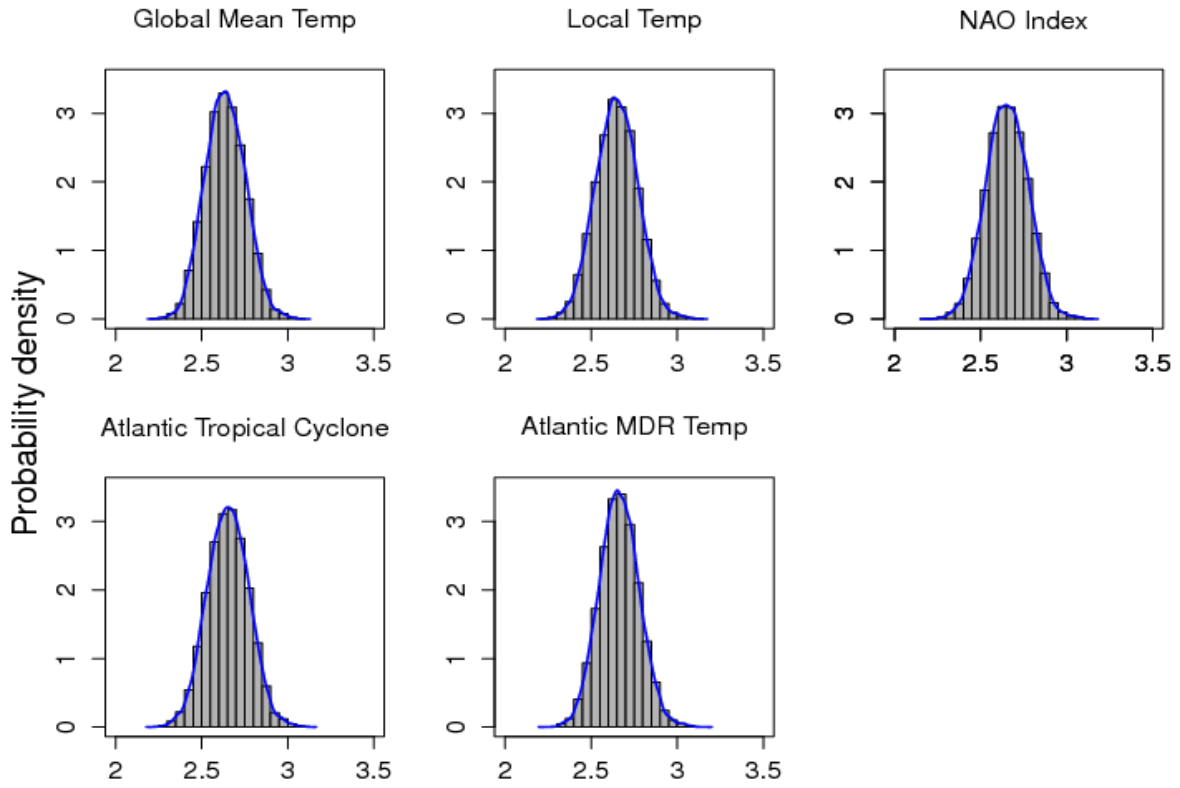


Figure S3: Posterior distribution in the regression parameter (intercept) for GEV nonstationary model for Baltimore/Washington International Thurgood Marshall Airport.

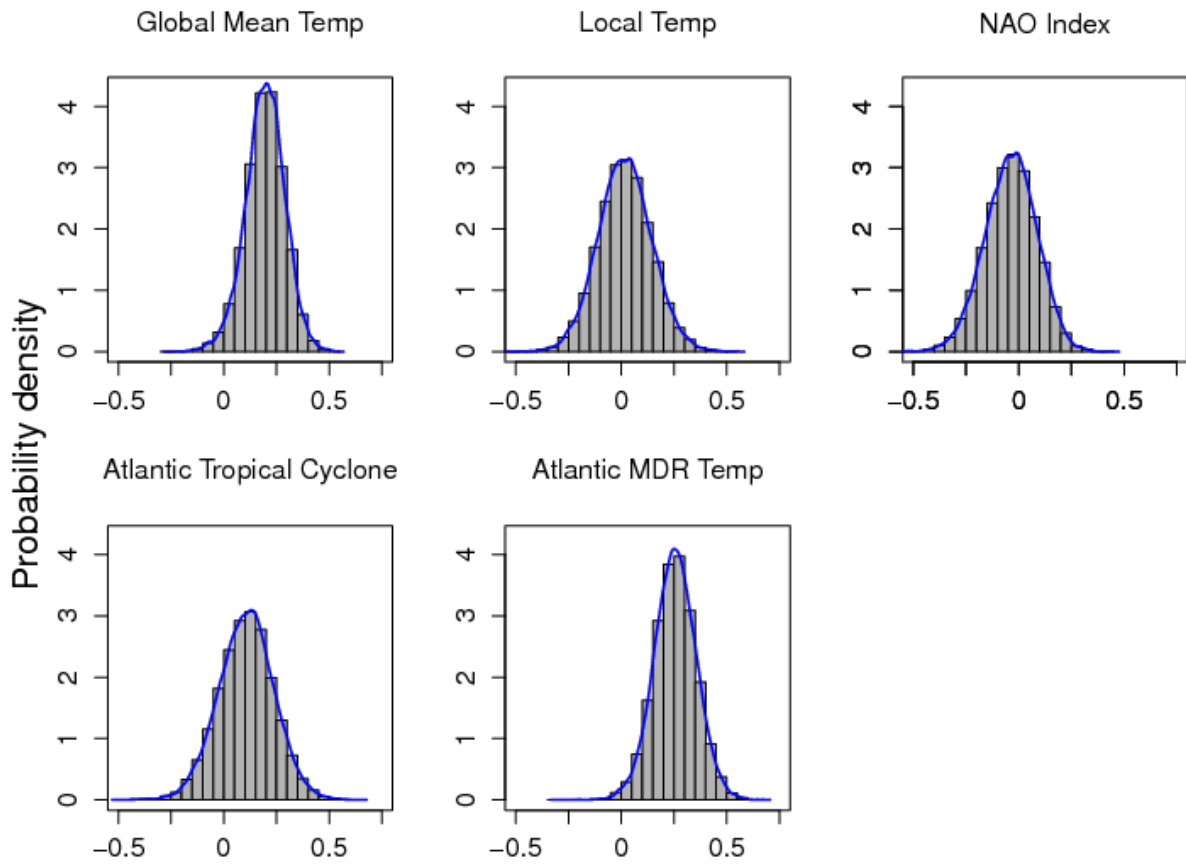


Figure S4: Posterior distribution in the regression parameter (slope) for GEV nonstationary model for Baltimore/Washington International Thurgood Marshall Airport.